Available online at www.sciencedirect.com
SCIENCE DIRECT
Tectonophysics 417 (2006) 53–68
TECTONOPHYSICS
www.elsevier.com/locate/tecto

# Spatio-temporal stress states estimated from seismicity rate changes in the Tokai region, central Japan

Shinji Toda [a,*], Shozo Matsumura [b]

[a] Active Fault Research Center, Advanced Industrial Science and Technology (AIST), Site 7, Higashi 1-1, Tsukuba 305-8567, Japan
[b] National Research Institute for Earth Science and Disaster Prevention (NIED), Tennodai 3-1, Tsukuba 305-0006, Japan

Received 26 August 2004; accepted 8 August 2005
Available online 10 January 2006

**Abstract**

Since unprecedented large-scale silent slip was detected by GPS in 2001 in the Tokai region, evaluating whether such movement is uniquely connected to the expected Tokai earthquake or repeatedly occurs in this area becomes vitally important. Because of short history of GPS observations and the limited areal coverage surrounding the Suruga trough, we take advantage of continuously recorded seismicity that is presumed to be sensitive to the deformation at seismogenic depth. Together with the well-maintained NIED earthquake data, we employ the seismicity-to-stress inversion approach of rate/state friction to infer the spatio-temporal stress changes in and around the presumed hypocentral zone of the future Tokai earthquake. Mapping stress changes inverted from microseismicity year by year, we find that the stress under Lake Hamana, the western expected future Tokai source, has been decreasing since 1999, during which the GPS data showed a normal trend of plate coupling. In contrast, stresses in the surrounding regions are calculated to have increased by transfer from Lake Hamana region. We interpret that this continuous process is associated with the 2000–2004 Tokai slow slip event. The characteristic patterns related to aseismic stress-release are also identified in the early 1980s and during 1987–1989, when slow events are inferred to have occurred on the basis of conventional geodetic measurements. Revisiting the seismotectonics and taking into account the mechanical implications of the inversion results, we argue that the transition zone situated between a deep stable creeping zone and a locked zone undergoes episodic creep and plays an important role in the transfer of stress to the locked zone. Consequently, even though we speculate that the current (2000 to present-day) silent slip event might be one of the repeating events, the inferred enlargement of the stress releasing area is significant and possibly raises the likelihood of the next Tokai earthquake.


*Keywords:* Tokai earthquake; Earthquake prediction; Stress change; Seismicity; Aseismic slow slip

## 1. Introduction

During the past decade, space geodesy revealed silent but extensive movement of the crust. The Tokai region of central Japan, one of the most densely monitored areas in the world because of the anticipated "Tokai M~8 earthquake," is now showing such unusual silent crustal movement (Fig. 1). An unprecedented deep silent slow slip event has been detected since 2001 (Ozawa et al., 2002) owing to the dense GPS network deployed by the Geographical Survey Institute (GSI) since the mid-1990s. Assuming the aseismic slip is causing the southeastward surface motions opposite to the normal northwestward motion, Ozawa et al. (2002) modeled the progression of slip along the plate interface. The aseismic slip event is still active in early

* Corresponding author.
*E-mail addresses:* s-toda@aist.go.jp (S. Toda), shozo@bosai.go.jp (S. Matsumura).

0040-1951/$ - see front matter © 2005 Elsevier B.V. All rights reserved.
doi:10.1016/j.tecto.2005.08.030

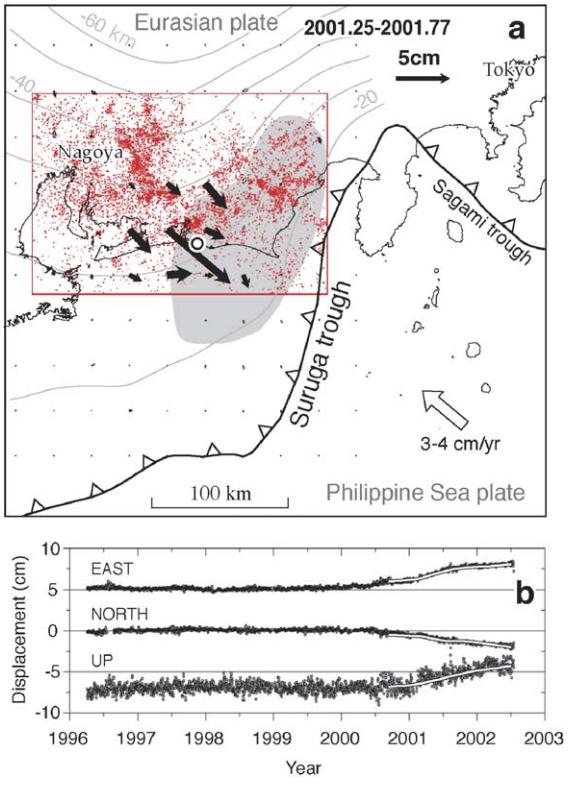


Fig. 1. (a) Interplate slow slip during 2001.25–2001.77 in the Tokai region estimated from GPS data (Ozawa et al., 2002). Arrows indicate slip vectors along the plate interface between the overriding Eurasian plate and subducting Philippine Sea plate. This interface is represented by gray contour lines. The shaded area indicates the source region of the future Tokai earthquake hypothesized by the CDMC (2001). Red dots indicate distribution of $M \geq 1.5$ earthquakes at depths of 20–80 km during 1979–2003 from NIED, used for the earthquake-stress inversion. (b) Detrended GPS time series recorded east of Lake Hamana (marked as an open circle in (a)) from Ozawa et al. (2002). The departure from the long-term trend is evident from late 2000.

2004; thus far, the total moment release has reached $5 \times 10^{19}$ Nm (roughly equivalent to a Mw=7.0 earthquake) (Geographical Survey Institute, 2004). This event is now spurring research and causing the government to reconsider the framework and rationale for the expected Tokai earthquake.

The Tokai region is located along the densely populated main route of traffic of the Pacific Coast in the heart of the industrial area connecting the Tokyo metropolitan district, Nagoya, Kyoto, and Osaka. Here, the Philippine Sea (PHS) plate located offshore is moving northwestward at ~3–4 cm/year and subducting beneath the Eurasian (EUR) plate. The subduction along the Nankai and Suruga troughs has been responsible for large mega-thrust earthquakes such as 1944 $M$=8.0 Tonankai and 1946 $M$=8.1 Nankaido earthquakes with 100–200-year inter-event times (e.g., Ando, 1975). The northernmost subduction boundary is the Tokai region; it did not rupture during the most recent 1944 Tonankai earthquake, and was identified as a large seismic gap in 1970s (Ishibashi, 1976). Since then, "the Tokai earthquake," uniquely named before its occurrence, has been one of the major targets in the Japanese earthquake prediction program (see detail review in Ishibashi, 1981; Yoshida, 2001). During the long waiting period, we have accumulated huge amounts of seismic, geodetic, and other geophysical data. Together with the experimental and theoretical studies about the dynamics of fault friction (e.g., Ohnaka, 1992), the major hope of the Tokai prediction is to rely on detectable precursory acceleration from preparatory slow creep leading to dynamic instability and failure (e.g., Kato and Hirasawa, 1999; Kuroki et al., 2002). This expectation is based, in part, on the observation of abnormal leveling data prior to the 1944 Tonankai earthquake (Ando, 1975). However, in the intervening 60 years since the Tonankai event, no such precursory deformation has since been observed for any subduction earthquake in Japan, despite today's far better geodetic monitoring.

Given the intense focus on the Tokai prediction, the 2000–2004 slow slip event raises a fundamental question for the Tokai earthquake forecasting. Is this slow slip event a unique–and thus possibly precursory–phenomenon in the subduction interface? To answer this question, we need to examine the behavior of the plate interface going as far back in time as possible.

The GPS data suffer from the short observation period (since mid-1990s). Even though the GSI has continuously surveyed the crustal deformation using conventional methods (leveling, triangulation, etc.) for a century, the data do not allow us to estimate the short-term motions discovered by GPS analysis. The GPS data can only detect moderate-to-large slippage if it occurs at seismogenic depths. Thus, using geodetic data alone, we cannot judge whether the slow slip event is unique to the 2000s and whether it can be directly associated with the anticipated future Tokai earthquake.

Micro-seismicity could also be an expression of strain and stress changes due to crustal motion at seismogenic depth. Recent studies of correlations between static stress changes and time-dependent seismicity rate changes furnish evidence for such associations. Seismicity is, at least in some circumstances, highly sensitive to tiny coseismic stress change such as one-tenth of the atmospheric pressure (e.g., Stein, 1999). Furthermore, changes in tectonic loading rate can also alter the

rate of small earthquakes over time (Toda et al., 2002). Thus, we expect that time series of microseismicity can be used as an in situ stress sensor to estimate crustal movements that are too small for the surface GPS network to detect until the cumulative movement becomes sufficiently large. The Tokai microseismicity time series is also longer than the GPS series, because the NIED has maintained the same detection level for the past 24 years, so that we can accurately evaluate seismicity rate change.

In this study, we first estimate the long-term stressing history in the Tokai region by applying the earthquake-stress inversion technique developed by Dieterich et al. (2000) to the NIED earthquake catalog. Mapping the spatio-temporal changes of the inferred stress states on the plate interface and subducting slab, we not only find the stress changes associated with the 2000 event, but also stress perturbations in 1980s. In light of the Tokai region seismotectonics, we evaluate the repeatability of such aseismic slips and implication to the future Tokai earthquake.

## 2. Earthquake-stress inversion method

Since the several studies of the 1989 Loma Prieta and 1992 Landers earthquakes (Reasenberg and Simpson, 1992; Stein et al., 1992; Jaumé and Sykes, 1992; Harris and Simpson, 1992), numerous papers have revealed that coseismic stress changes can promote or inhibit local seismicity. Even though there are several unknown factors (the fault friction coefficient, pore pressure change, pre-existing fault orientations, random fluctuation of earthquake occurrence), can alter the stress change pattern, the spatial correlation between calculated stress changes and observed seismicity rate changes is generally high (Harris, 1998; Stein, 1999). In addition, recent efforts seek to extend this understanding by explaining the time-dependency of seismicity after one or multiple earthquakes strike (e.g., Toda and Stein, 2003), and stressing rate change (Toda et al., 2002) using the rate- and state-dependent friction law (Dieterich, 1994).

The correlation between static stress change and seismicity rate change as a function of space and time encourages us to use the microseismicity as a sensor of the crustal strain or stress. Dieterich et al. (2000) developed a technique to invert the local rate of earthquake occurrence to static stress changes based on rate- and state-friction. They successfully reproduced stress steps and stressing rate changes in the dike intrusion processes at Kilauea volcano, which show good agreement with documented surface deformation. Under the condition that local microseismicity is continuously high and well recorded, their method provides a way to use seismicity rate information contained in earthquake catalogs as a stress meter. This criterion is well satisfied by the NIED catalog in Tokai region.

The formulation to determine the seismicity rate in the stress fluctuation process, after Dieterich (1994) and Dieterich et al. (2000), can be given by

$$R = \frac{r}{\gamma \dot{S}_r} \tag{1}$$

where $\gamma$ is a state variable directly altered by stress changes, $\dot{S}_r$ is a loading rate of Coulomb stress under the background steady state seismicity rate $r$. The state variable $\gamma$ is resolved with time $t$ as

$$\mathrm{d}\gamma = \frac{1}{A\sigma}\left[\mathrm{d}t - \gamma \mathrm{d}S\right] \tag{2}$$

where $A$ is a dimensionless fault constitutive parameter (normally in the range 0.005–0.015, as summarized in Dieterich et al., 2000), $\sigma$ is effective normal stress, and $S$ is Coulomb stress.

The time to return to a steady state of seismicity after a perturbation is defined as

$$t_a = \frac{A\sigma}{\dot{S}_r}. \tag{3}$$

The burst of seismicity is due to a sudden stress step caused by a nearby earthquake, in which seismicity gradually decays following the typical Omori's aftershock law and lasts a certain period expressed the aftershock duration $t_a$. So, under constant $A\sigma$, aftershock duration $t_a$ is inversely proportional to the stressing rate $\dot{S}_r$.

The spatial distribution of stress changes ($\Delta S$) as a function of time can be resolved with the solution of Eq. (2) for an initial assumption of constant Coulomb stressing rate $\dot{S}_r$ defined from the other parameter assumptions in Eq. (3). In order to seek $\Delta S$ from the observed time-dependent seismicity rate, the earthquake catalog is used for counting earthquakes in a certain time interval. Assuming a constant stressing rate at $\dot{S}_r$, a stress step $\Delta S$ is expressed as

$$\Delta S = A\sigma \ln\left\{\frac{\dot{S}\left[\exp\left(N_2\dot{S}_r t_1/N_1 A\sigma\right) - 1\right]}{\dot{S}_r\left[\exp\left(\dot{S}t_2/A\sigma\right) - 1\right]}\right\} \tag{4}$$

where $N_1$ is the number of earthquakes in time interval $t_1$ immediately before the stress event, and $N_2$ is the number of earthquakes in interval $t_2$ immediately after the event. $\dot{S}$ is Coulomb stressing rate assumed from Eq. (3). This equation can not only calculate the stress

step between the time steps but also the stressing rate change indirectly from a series of small stress steps in a given time period.

## 3. Data and assumptions

We use $M \geq 1.5$ earthquakes at depths between 20 km and 80 km to invert stress state; these shocks are mainly in the subducting PHS plate. Matsumura (1997) reveals the distribution of seismicity in the overriding EUR plates and subducting PHS plate, whose boundary roughly corresponds to the 20-km upper limit except offshore areas, which we do not analyze. The minimum magnitude of completeness (Mc) during the past 25 years for the NIED catalog is estimated to be 1.5 from thorough examinations by Matsumura (1997) and Wiemer et al. (2005). Due to highly clustered shallow seismicity in the EUR (Fig. 5 in Matsumura, 1997), we focus on the PHS seismicity, most of which are deeper than 20 km (Fig. 1).

We first count earthquakes in numerous sub-regions in the subducting PHS slab. To map the detailed stress states, we divide our study area into 1350 4-km-square-by-60-km-deep cells. At the center of each cell, we initially set a cylinder that has 2.83-km radius (4 km $\times\sqrt{2}/2$ km; see Fig. 2a) covering the entire squared cell to collect enough earthquakes for the stress history estimation. For the sampling process, we enlarge the radius to collect a certain number of shocks. There is a trade-off between minimizing uncertainty for the inverted stress and enlarging the areas, so we set the minimum number of shocks per year to be five in our inversion. Accordingly, we change the radius step by step to satisfy the condition of $\geq 5$ shocks until the cylinder reaches a maximum radius of 14.14 km (~five neighboring cells shown in Fig. 2a). A cell rejected from this condition is mapped as undefined and is not color-coded (undefined area in Figs. 3 and 4). For the rate- and state-dependent friction parameters in the equations, we assume $t_a$ is 1 year, since aftershocks of the moderate-size earthquakes in this region do not seem to persist for more than 1 year (e.g., one in Fig. 2). Another parameter $A\sigma$ is normally assumed to be 0.4–1.0 bars based on laboratory measurements of $A$, waveform inversion and empirical relations between coseismic static stress changes and seismicity rate changes (summarized in Toda and Stein, 2003). Here for simplicity we assume $A\sigma = 1$ bar, but the overall tendency of the stress curves would not be changed because dimensionless stress is assigned to the $y$-axis. From Eq. (3), both assumed parameters imply an initial tectonic loading rate of 1 bar/year, which provides a reasonable 100-bar stress drop with a 100 year interevent time under the condition of full plate coupling.

To display the stress history from all cells, we present two types of maps. One shows the distribution of annual Coulomb stress increments (Fig. 3). The other shows changes in the Coulomb stressing rate (Fig. 4). On a stress curve (e.g., a red line in Fig. 2), the first map plots the increment needed to subtract the amount of Coulomb stress accumulated at 1 year from the next year (the amount of stress between A′ and A in Fig. 2).

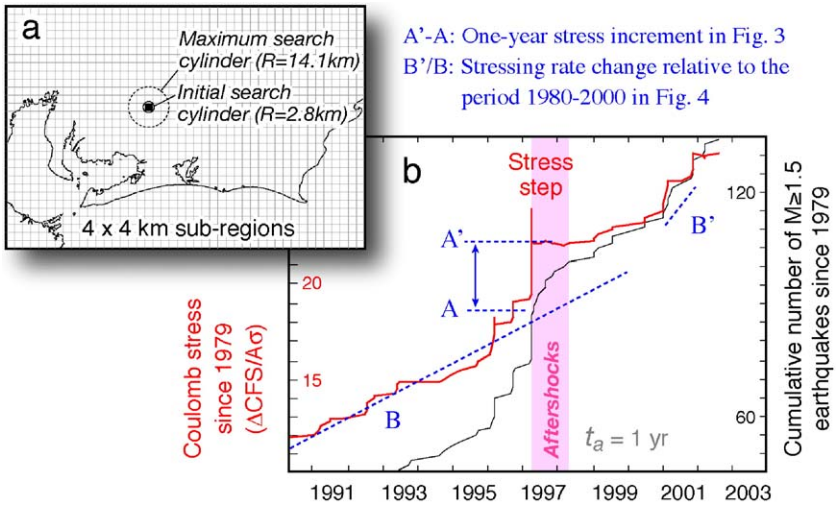


Fig. 2. (a) Matrix of cells analyzed to infer stress from seismicity. (b) Cumulative number of earthquakes (black line) and calculated stress accumulation process (red line) as a function of time at a solid square region in (a). A stress step is revealed in this sub-region. One-year stress increments (e.g., A′–A) for all sub-regions are mapped in Fig. 3, whereas the change in 1-year stressing rates from the long-term rate (e.g., B′/B) is shown in Fig. 4.

This approach is useful to detect local stress steps. Unlike conventional mapping of the calculated Coulomb stress change, these maps have a positive stress-change (e.g., warm color) bias because of the annual 1-bar stress accumulation that occurs on top of the stress fluctuations. In addition, if seismicity rates are low or near-zero, seismicity rate increases are more readily measured than decreases. Consequently, the white-to-blue areas suggest Coulomb stress drops or regions in which the process of stress loading has stagnated. The second type of map (Fig. 4) displays the annual change in the Coulomb stressing rate relative to the average long-term background in the period between 1980 and 2003. For example, in Fig. 2, slope of the stress curve in 2001 (B′) is compared with the background slope (B) and then colors are coded in log stressing rate change. So here, the blue areas do not necessarily imply a net stress decrease but rather a stressing rate less than the loading rate. In addition to the maps, we calculated time series of stress for particular cells to examine their inferred stressing histories (Fig. 5).

## 4. Results

A stress shadow corresponding to the 2000s Tokai slow slip event is evident just under Lake Hamana

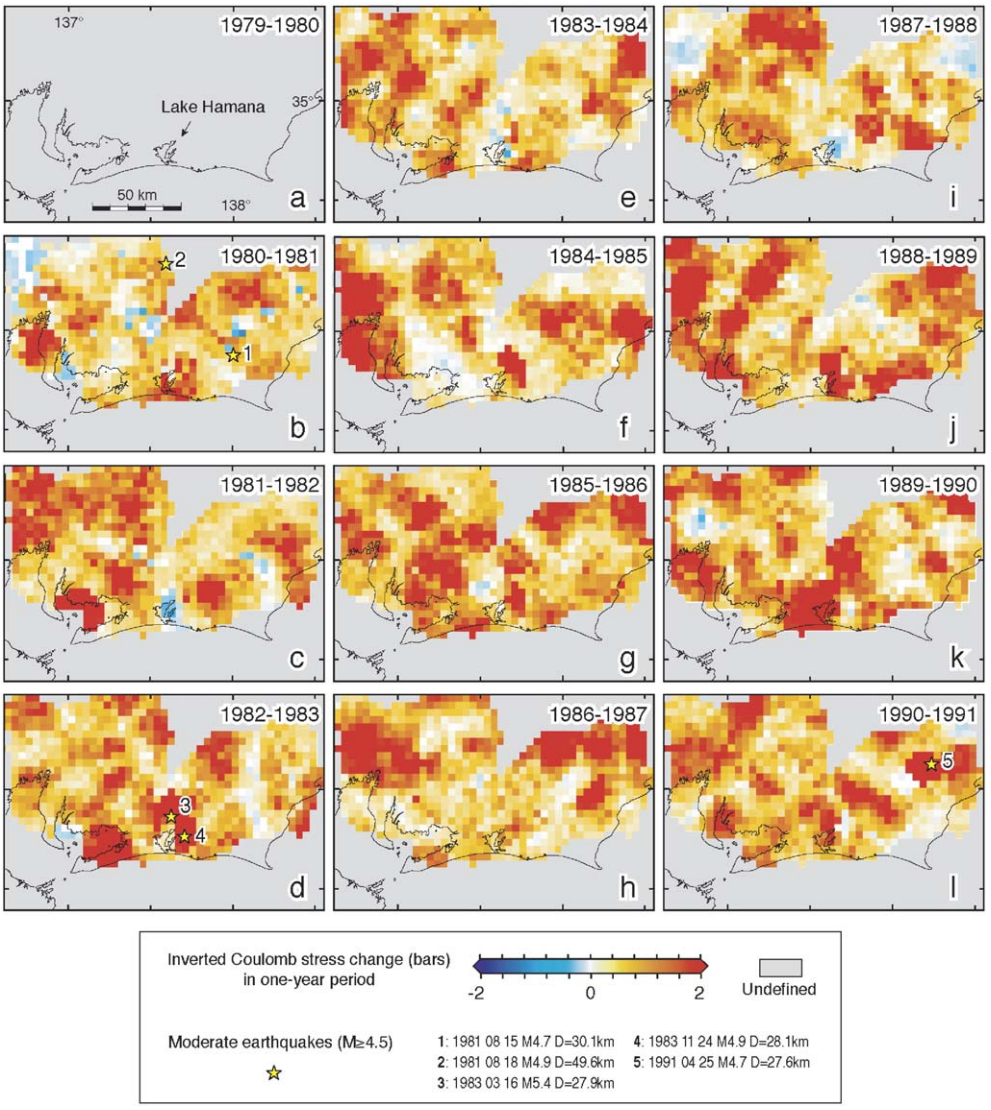


Fig. 3. Annual Coulomb stress change inverted from seismicity rate in each sub-region. The average annual stress increase is set to be 1 bar, so that the color images are biased toward warm colors. Nevertheless, many areas are calculated to have experienced stress decreases. Catalog incompleteness of the initial NIED network renders the first period undefined.

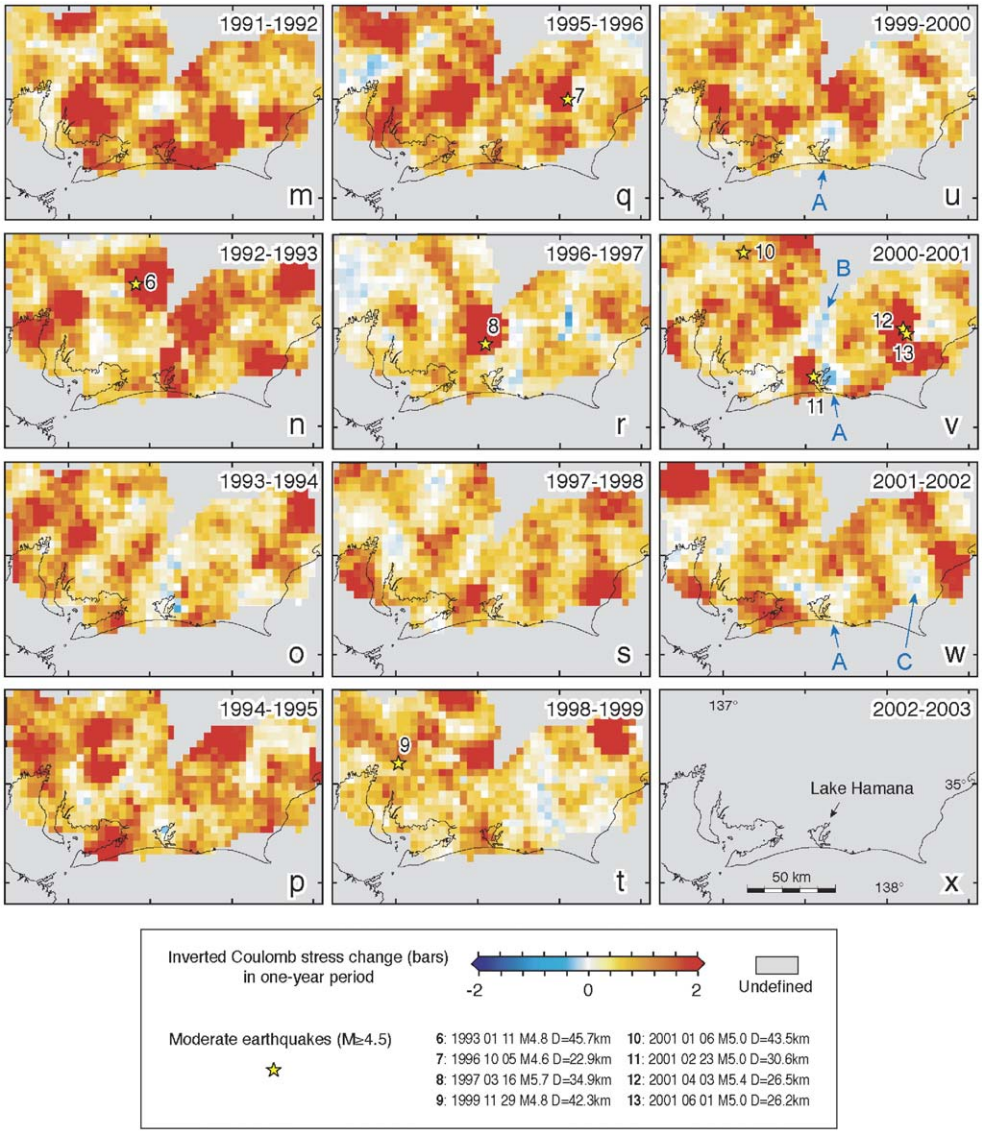


Fig. 3 (*continued*).

during 1999–2000 to at least 2001–2002 (Fig. 3u–w, site A). The inferred stress decrease started northeast of Lake Hamana in 1999–2000 (Fig. 3u, site A) and expanded to the north in 2000–2001 (Fig. 3v, site B). This evolution of the stress shadow resembles the gradual expansion of the slow slip area estimated by Ozawa et al. (2002) from GPS analysis. In the plots of the stressing rate change, the stress shadow is more pronounced, and in addition to the Lake Hamana region (Fig. 4v–x, sites A and B), there is also a feature near the proposed source region of the future Tokai earthquake (Fig. 4v–x, site C). Moreover, the unloading or stress decrease phase under Lake Hamana seems to have started in 1998–1999 (Fig. 4t) that is not as clearly detected in Fig. 3 due to the overprint of secular stress loading. It is also plausible to infer that anomalous unloading had been gradually occurring at the Lake Hamana region and other areas since 1995–1996 (Fig. 4q).

Several moderate-size earthquakes might have been triggered by stress transfer from the aseismic slip under Lake Hamana. An annulus of Coulomb stress increase encloses the stress decrease area under Lake Hamana in 1999–2000 (Fig. 3u), although the change in the stressing rate in Fig. 4 is not distinct, possibly due to averaging. In the next time period, 2000–2001, three $M=5$ shocks occurred in areas surrounding the stress shadow. This leads us to infer that the earthquakes were

promoted by stress increases that ringed the slow slip zone. Note that the stress steps and related stress loading produced by such moderate shocks lasted a few years, gradually shrinking (Fig. 4v–x).

Our inversion analysis suggests that similar types of aseismic slip might have occurred in two distinct periods of 1981–1984 and 1987–1989. Compared to the relatively stable loading in the 1990s, significant stress shadows under the Lake Hamana region can be inferred in the 1980s (1981–1982, 1983–1984, and 1987–1988 in Fig. 3; 1981–1985 and 1987–1989 in Fig. 4). Although these stress decreases might not have lasted as long as the one in the 2000s, the inferred stress changes are comparable in magnitude. Additionally, the locations and NW-expansion pattern in Fig. 4 are similar to those of the 2000s.

Three inactive periods are identified on the Lake Hamana time histories (Fig. 5) that resemble the subsequent 2000–2004 slow slip event. Further, the initiation of the 2000 slow slip event can be dated back to the late 1990s (at the earliest 1996 and at the latest 1999) before the GPS anomaly (Ozawa et al., 2002) began. The stress curve in cell 1 (colored blue) located west of Lake Hamana shows constant stress loading without any stress perturbations. Stresses in three cells (3, 4, and 5 in Fig. 5) underlying Lake Hamana demonstrate significant stress fluctuations with distinctive stress decreases and sluggish accumulations in the periods

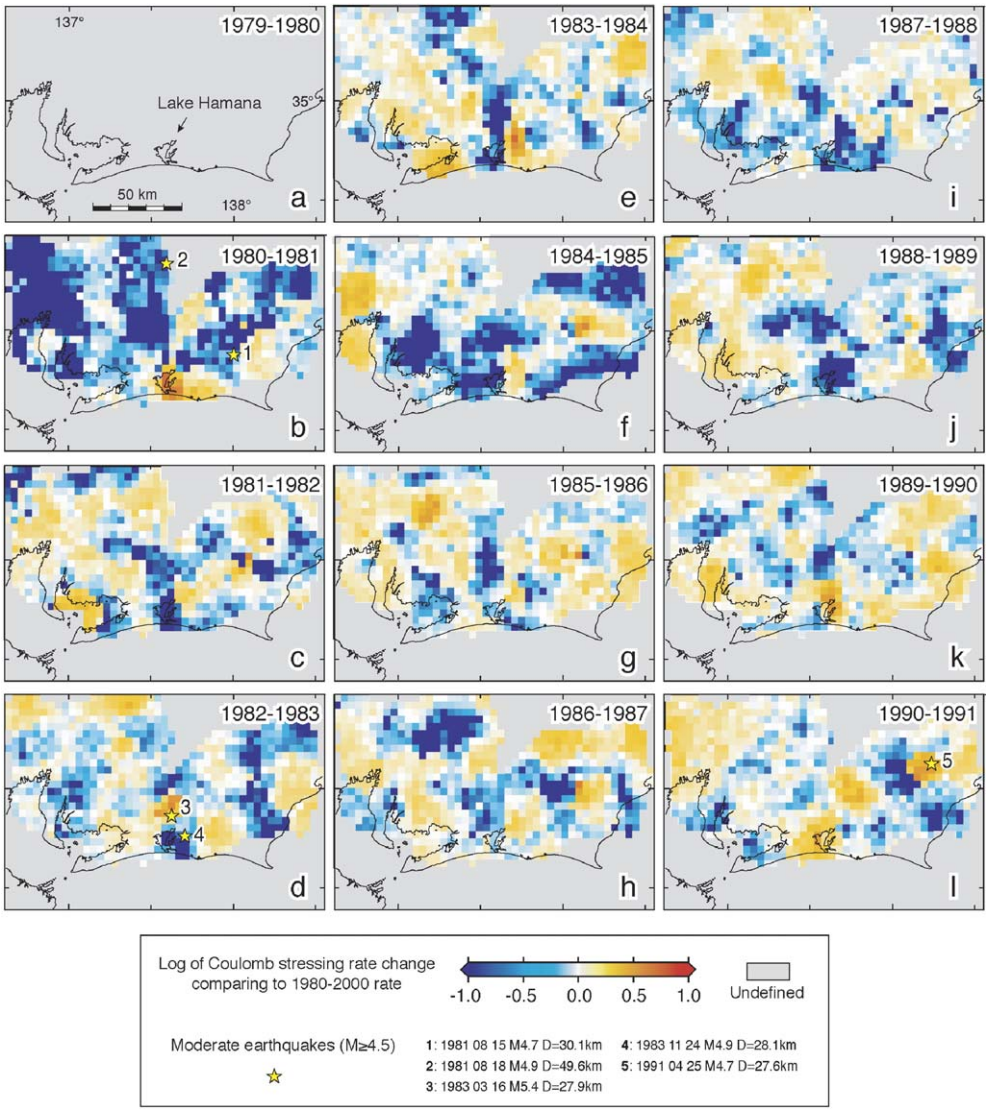


Fig. 4. Change in Coulomb stressing rate compared to the long-term rate averaged for the period 1980–2000 (note the log scale). Unlike the stress increments in Fig. 3, the white color indicates average or secular stressing, whereas red and blue present a rate increase and decrease, respectively.

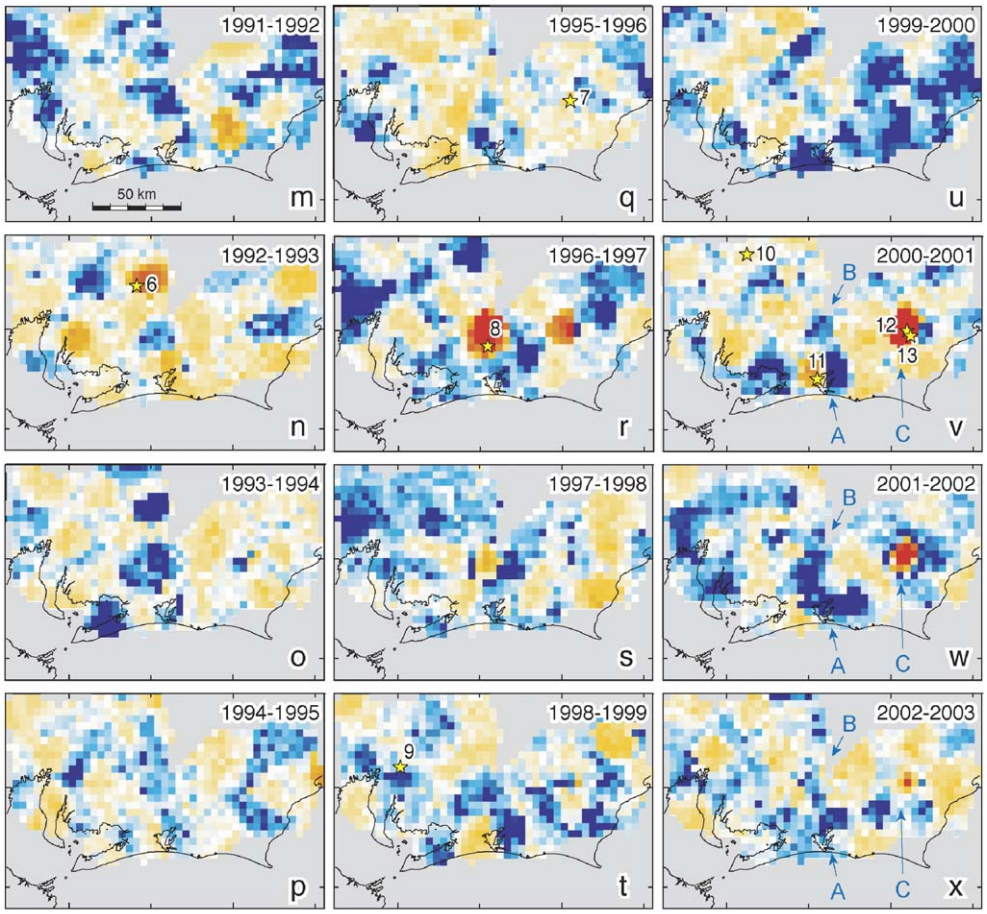


Fig. 4 (*continued*).

shown in gray. It is noteworthy that moderate-size earthquakes that occurred in the early 1980s might also have been triggered during the aseismic events. They show only step-like stress increases in the dormant period.

Our suggestion of possible slow slip events in the 1980s, however, is not the first discovery in the Tokai region. Kimata et al. (2001) proposed silent slip events took place in the 1980s based on changes of the EDM baselines and leveling data. They suggested the relative cessation of shortening of two baselines (L1 and L2 in Fig. 7) as a result of slowed back-slip relative to the normal 3–4 cm/year rate. Although their two periods do not perfectly agree with our estimates from microseismicity, these inferences are from independent data and analyses. Thus, we conclude that two distinct periods of stress shadows were indeed related to the aseismic slow slip events centered at the Lake Hamana region.

## 5. Discussion

Our earthquake-stress inversion suggests that there was a stress release in a portion of the plate interface and a stress increase in the surrounding region. But we implicitly assume all the earthquakes used for the analyses are nearly optimally oriented in the uniform tectonic stress regime in the Tokai region, where the compressional stress axis is NW–SE parallel to the

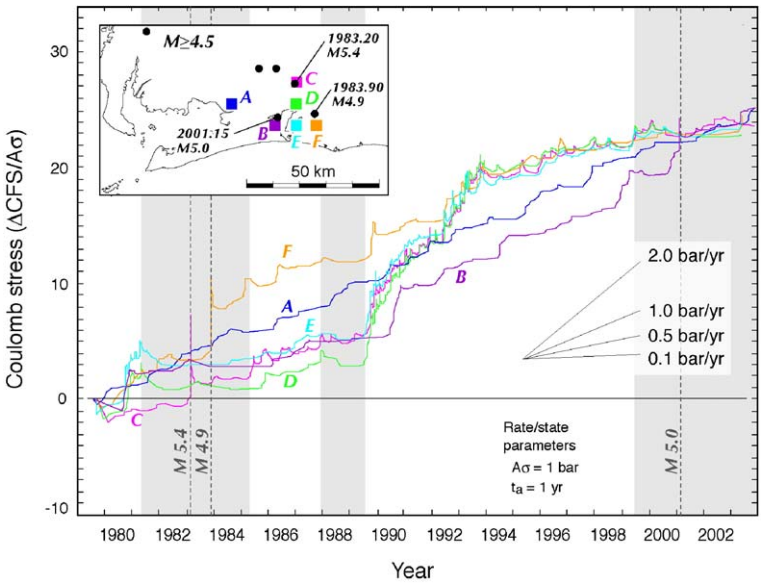


Fig. 5. Several examples of Coulomb stresses estimated from seismicity rates near Lake Hamana. The inset shows the distribution of the sub-regions, along with moderate-size earthquakes that produced some of the observed stress steps. Three epochs of inferred stress decrease are indicated as shaded zones. Sites C, D, and E also experience accelerated stressing during mid-1989–mid-1993.

northwestward movement of the PHS plate. As seen in forward models for Coulomb stress analysis, inverted stress change values strongly depend on fault strike, dip and rake (slip direction). Thus, we must also consider the types and orientations of faults on which the stress changes are resolved.

Because of the curvature of the plate boundary, the effect of collision of the Izu Peninsula, and the segmented structures of the plate interface, as discussed by Ukawa (1982, 1991), the stress field in the Tokai region is not straightforward. Despite the expectation that a majority of earthquakes in the Tokai region are thrust events due to strong seismic coupling, strike-slip and normal faulting earthquakes are abundant (Matsumura, 1997). In addition, the focal mechanisms are not the same throughout the entire Tokai region and show some diversity influenced from local stress heterogeneity and crustal structure. Furthermore, without understanding the tectonic situation that produces the microseismicity, we cannot speculate on the implications for the future Tokai earthquake occurrence due to the slow slip event. We therefore need to revisit the seismotectonics in Tokai region.

### 5.1. Seismotectonics revisited

To see the framework of the Tokai region, we first create eight seismic cross-sections oriented parallel to the convergence direction of the two plates (left panels in Fig. 6, corresponding locations are in Fig. 7). In all but section Fig. 6a, two seismic layers, a flat shallow band of seismicity and a NW-dipping one, are recognized, corresponding to the overriding Eurasian plate and subducting Philippine Sea plate. The seismically visible leading edge of the PHS plate reaches deeper to the southwest (Fig. 6b to h). In the most eastern section (Fig. 6a), we cannot observe the subducted slab, which is interpreted to be a plate collision zone (e.g., Ukawa, 1991). Sections in Fig. 6b–e are typical of subducting slab geometry which dips 10–20° to the northwest and upward-convex (upward-bending) shape in the deeper portion. The dip and the bending mode in the section change between sections in Fig. 6e and f. The dip becomes shallower and the slab is characterized by un-bending deformation a convex-upward shape. Accordingly, in the northwestern part of the sections in Fig. 6g and h, it is hard to distinguish intra-slab events from scattered shallow seismicity. Such changes of the subducting PHS plate shape and dip indicate that stress acting on the slab is not homogeneous and some localized forces can be expected due to the plate bending, stretching and unbending.

There are two remarkable features of the seismic coupling zones where the PHS plate subducts beneath EUR (Fig. 6). One is the deep seismic cluster at the bottom of the EUR seismogenic layer (Fig. 6d–e, at a distance of 100–130 km and depth of 20–25 km). The other significant feature is an aseismic zone (the zone

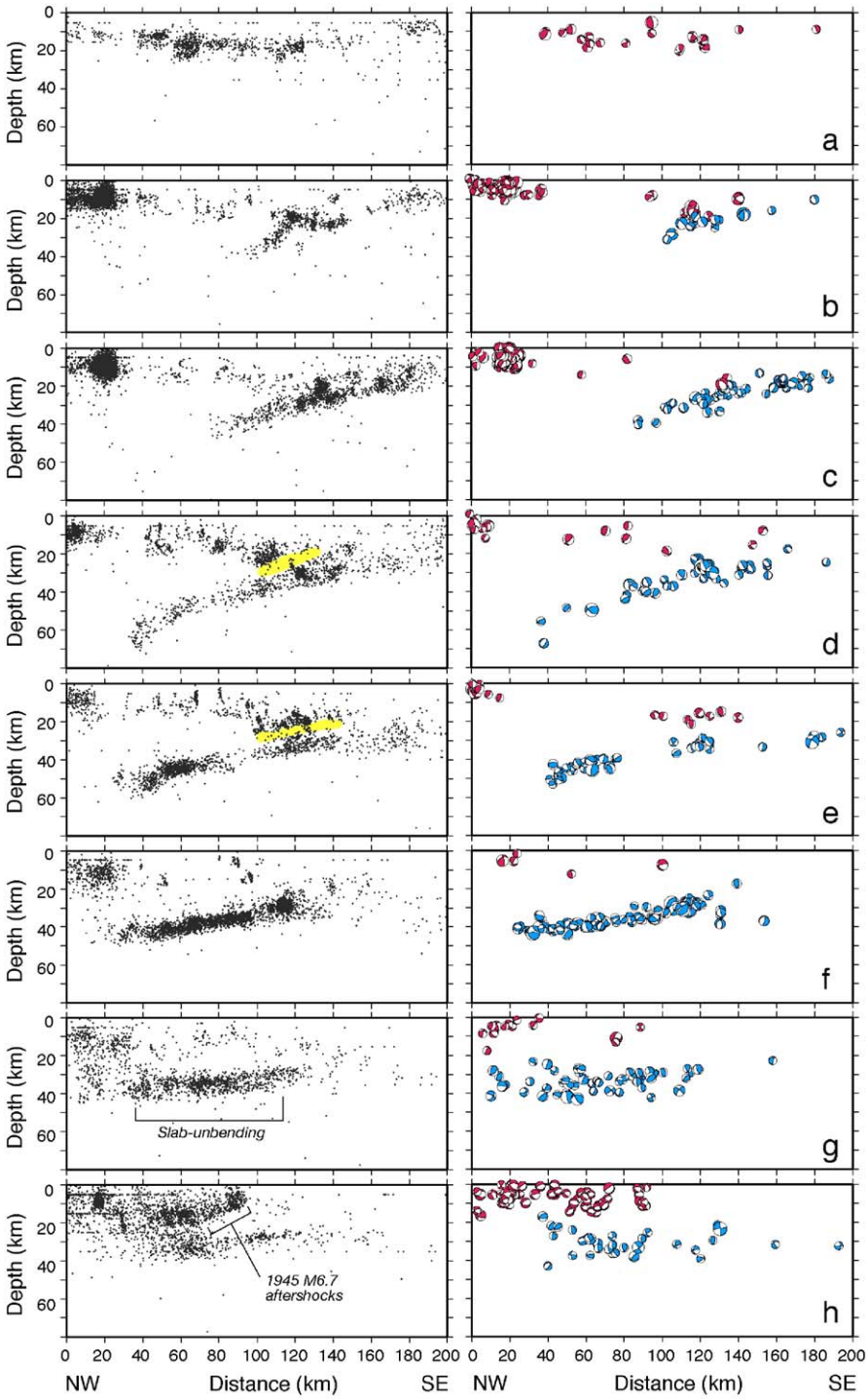


Fig. 6. Distributions of 1979–2002 $M \geq 1.5$ hypocenters (left panels) and side projections of well-determined NIED focal mechanisms for $M \geq 3$ earthquakes (right panels) in cross-section, corresponding to sub-areas a–h in Fig. 7. Presumed changes in subducted-slab dip and down-dip extent along the strike are visible. The yellow band in left panels d and e are aseismic but presumed to be locked, sandwiched by highly active earthquake clusters. Focal mechanisms are from (http://www.bosai.go.jp/center/kanto-tokai/data/indexm.html). Most of the intra-slab events show strike-slip and normal earthquakes. Thrust earthquakes are rarely observed in the shallow plate coupling zones.

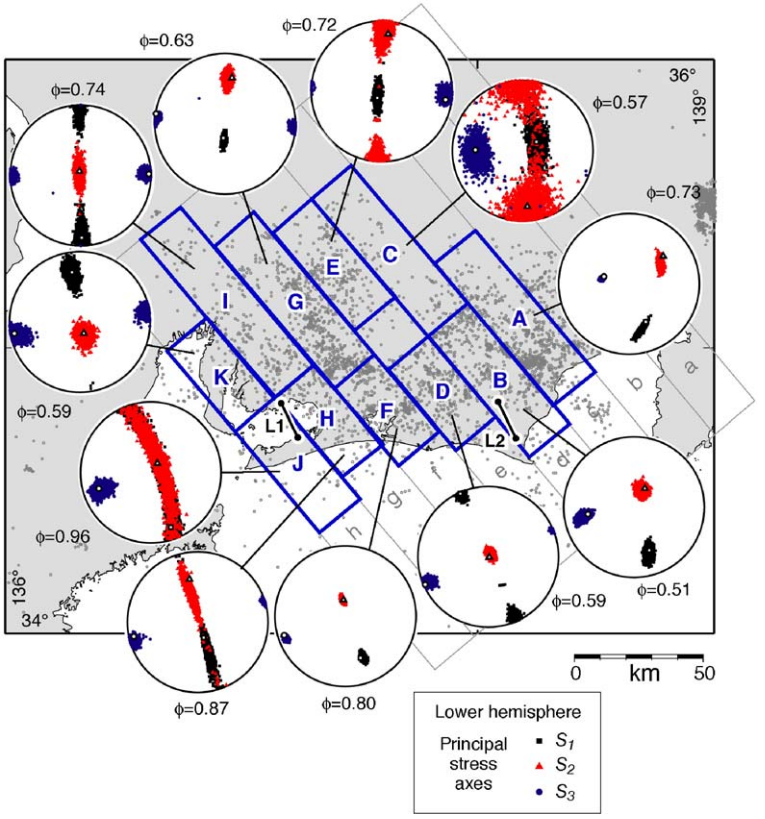


Fig. 7. Principal stress axes in the subducting slab estimated from stress tensor inversion using the NIED focal mechanisms ($M \geq 0$, 1979–2002, depth: 20–80 km). Bootstrap resampling (2000 times) following Michael (1987) is used for the inversion in the program ZMAP (Wiemer, 2001). The shape of the deviatoric stress ellipsoid, defined by $\phi$ of Angelier (1979), is also calculated for each sub-region. Although there might be some temporal changes in the focal mechanisms (e.g., Wiemer et al., 2005), here we do not consider time-dependency because it would greatly reduce the number of analyzed shocks. Gray colored boxes are corresponding to the ones for the seismic cross-sections in Fig. 6. Locations of the EDM baseline lengths that Kimata et al. (2001) used for the changes in distance are shown as orange lines.

lacking in microearthquakes, shown by the yellow band in Fig. 6d–e) sandwiched between the dense clusters of earthquakes in EUR and intra-slab shocks. This aseismic characteristic might be attributable to two things: The uppermost PHS is largely aseismic farther offshore, and might remain aseismic even as it subducts beneath EUR. The other is that stress may concentrate on the plate interface located between stable sliding zone and coupling zone. Together with the dense clusters of seismicity at the base of EUR, these observations suggest that strong kinematic coupling of the two plates produce such a clear contrast of seismicity, locally deepening the base of the seismogenic layer.

Well-determined focal mechanisms enhance the inferences drawn from the seismic cross-sections by permitting us to estimate the stress field acting in the subducting slab (right panels in Fig. 6). It is significant that stress fields in the EUR and PHS plates are quite different. Most focal mechanisms in the overriding EUR plate are strike-slip or reverse, whereas those in the PHS are strike-slip and normal. Further, *P*-axes are oriented E–W in the overriding plate, whereas *P*-axes in the PHS are oriented NNW–SSE (Matsumura, 1997). Thus, most shallow inland shocks in the EUR plate have been occurring with little or no influence of the coupling with the PHS.

In-depth information on stress tensors is more revealing for the PHS and EUR stress state than simple *P*- and *T*-axes moment tensors shown in Fig. 6. We perform the stress tensor inversion for the principal stress axes using Michael (1987) bootstrapping approach implemented in the software, ZMAP (Wiemer, 2001), using all available NIED focal mechanism data (Fig. 7). Additionally, we calculate the shape of the deviatoric stress ellipsoid defined as

$$\phi = \frac{S_2 - S_3}{S_1 - S_3}, \tag{5}$$

where $S_1$ is the most compressional principal stress, $S_2$ is the intermediate principal stress, and $S_3$ is the least

principal stress (Angelier, 1979). Stresses in the subducting PHS plate are shown in Fig. 7. Except for the possible thrust-promoting stress field in the region A, most of the areas previously thought to be locked (e.g., Matsumura, 1997, sub-regions B, D, and F in Fig. 7) exhibit a strike-slip stress regime, whereas the inverted stress tensors in the down-dip extensions to the northwest (sub-regions, C, E, and G in Fig. 7) are instead compatible with normal faulting earthquakes. Sub-regions west of Lake Hamana indicate different stress regimes. Sub-regions H and J may have the same stress field with the ones in the eastern regions. The regions show high $\phi$ values, which indicate that $S_1$ and $S_2$ are so similar that their directions are nearly interchangeable. Consequently, regions located west of Lake Hamana can accommodate stress perturbations with constant seismicity. Overall, the direction of $S_3$, which might correspond to the along-strike stretching of the subducting slab (Ukawa, 1982), is rather stable, showing an E–W trend, whereas $S_1$ and $S_2$ directions are exchanged from the shallow to deeper portions of the eastern Tokai region, and are unstable in the western Tokai region.

### 5.2. Interpreting stress regimes

To explain the stress regime and focal mechanisms change within the PHS plate, we make a simple model to present changes in orientations in principal stress axes in the down-dip direction, building on the work of Matsumura (1997). Fig. 8 shows a cross-section of the two-state (locked and creeping) model in an elastic half-space (Okada, 1992). The model shows changes in the plunge angle of the principal $S_1$ and $S_2$ stress axe ($S_3$ is oriented nearly parallel to the PHS strike, or into the page of Fig. 8). First, the unsubducted offshore portion of the PHS plate typically produces pure strike-slip earthquakes. We thus set the initial $S_1$ plunge without any stress perturbation to be parallel to the plate interface. The locked section causes a strong perturbation of the stress field, vertically rotating $S_1$ and $S_2$. $S_1$ is oriented in the down-dip direction under the slipped zones, where normal faulting earthquakes are expected. In contrast, the dip of $S_1$ becomes close to horizontal beneath the locked patch, so we would expect pure strike-slip faulting earthquakes to occur. In the rest of the shallow plate interface, normal faulting earthquakes would be expected where stable sliding occurs.

Based on the analysis of microseismicity, focal mechanisms, stress tensor inversion, and dislocation modeling, we propose a new delineation of plate coupling for the Tokai region (Fig. 9). We regard the regions where episodic slow slip occurs as the transition zone between the completely locked portion and stable creeping zone. The transition is also characterized by the mixture of strike-slip and normal faulting focal mechanisms, represented by regions H and J in Fig. 7, in which we interpret the mixture of the mechanisms as the product of partial slow slip in a region that adjusts to any episodic stress disturbance. Our locked zone, similar to that of Matsumura (1997) except in the Lake Hamana sub-region, is much more confined than that of the Central Disaster Management Council of the Japanese government (CDMC, 2001). It is difficult to infer the coupling state close to the Suruga trough from microseismicity data, where CDMC (2001) identifies

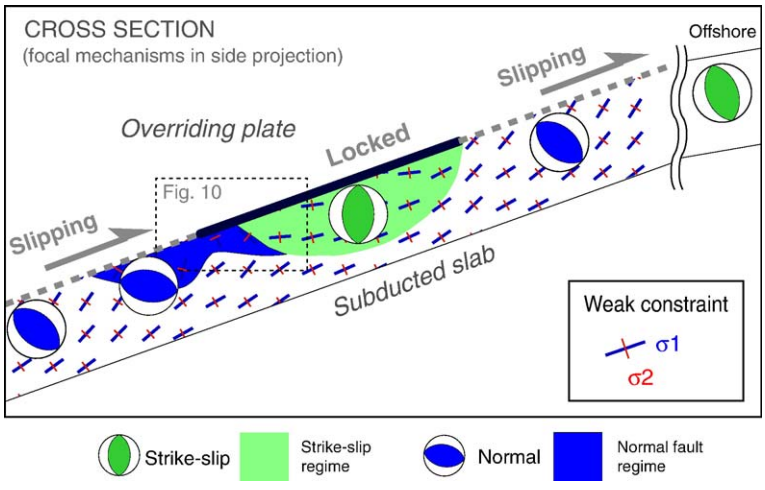


Fig. 8. Stress perturbation and focal mechanisms expected for a transition from a locked to a creeping plate interface. The $S_3$ axis is perpendicular to the plane of the figure and so is not shown.

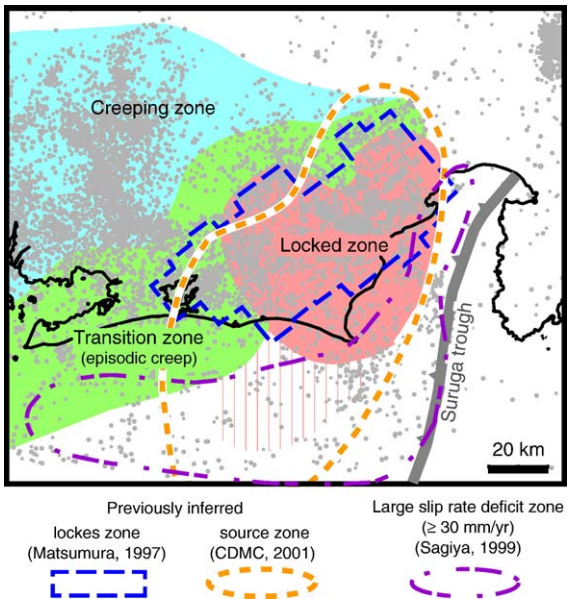


Fig. 9. Proposed distribution of slip on the plate interface, based on microseismicity, focal mechanisms, stress tensor inversion, and elastic modeling. The transition zone is characterized by the episodic creep (e.g., slow slip events).

the southwest extension of the source as a slip deficit based on studies of historical earthquakes.

Our transition zone is analogous to the Parkfield section of the San Andreas fault, since both transmit strain a region of stable sliding to seismogenic sources. In both cases, the fault partially creeps, has high microseismicity, and produces $M\sim6$ earthquakes every 20–40 years, accompanied with substantial postseismic creep. In the central to southern San Andreas, it is proposed that $M\sim8$ shocks such as the 1857 Fort Tejon earthquake might have been triggered by one of every several Parkfield-type shocks that were strained by the creeping section (Arrowsmith et al., 1997). If such a system commonly operates in the plate boundary and is mechanically reasonable, the expected Tokai earthquake would be more likely to occur during one of the aseismic events.

The substantial difference between our locked zone and the zone of high slip-rate deficit identified by Sagiya (1999) is a controversial issue. Land-based geodetic data have limited resolution to estimate the slip rate of the up-dip portion of the interface far offshore, and Sagiya's slip-deficit zone is almost entirely localized offshore. But we believe that a more fundamental contradiction derives largely from confusion about how best to interpret plate "coupling" (Wang, 2004) from geodetic data. Even though we infer a large slip deficit in the shallow part of the subduction, we do not know whether this part of the plate interface is kinematically strong or not. In other words, even though the most shallow part of the interface is weak, it does not slip freely because of the purely locked portion immediately downdip. Thus the large geodetically determined slip deficit extends into the high pressured fluid and soft sediments, which are unlikely to store enough stress to rupture

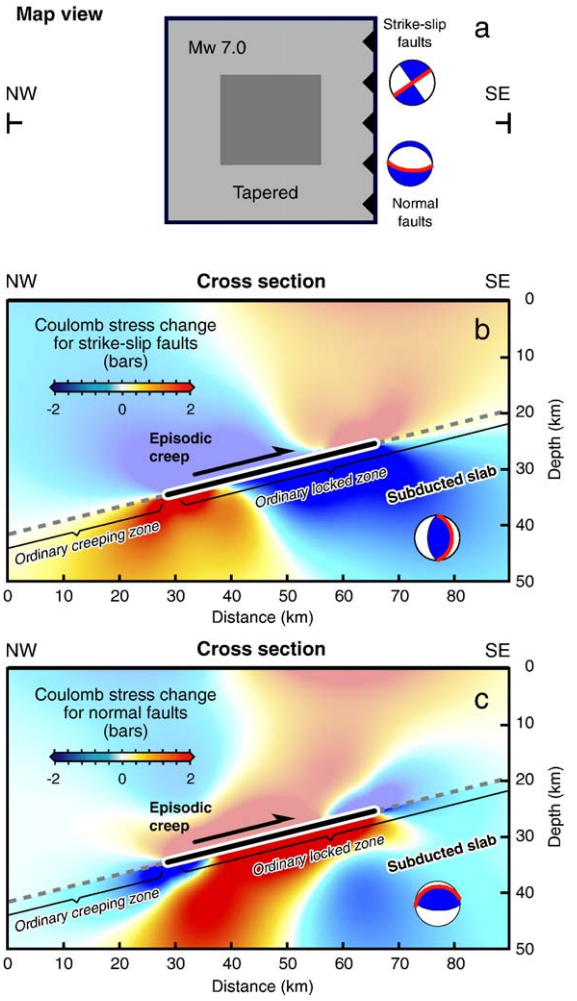


Fig. 10. Coulomb stress changes in cross-section for intra-slab earthquakes caused by a slow slip patch with a moment similar to which occurred since 2000. (a) Map view showing simplified thrust fault patch undergoing slow slip. The slip is linearly tapered from the edges of the dark gray uniform-slip central patch to the fault edges. The nodal plane on which stress change is resolved (red line) is represented on the map-projection of focal mechanism. (b) Coulomb stress change for strike-slip faults (represented by a red line in the side-projection of focal mechanism). Faults beneath the creeping patch are calculated to have moved farther from failure. (c) Coulomb stress change for normal faults beneath the creeping patch is calculated to have risen, whereas the stress in the down-dip of the creeping patch is calculated to have dropped.

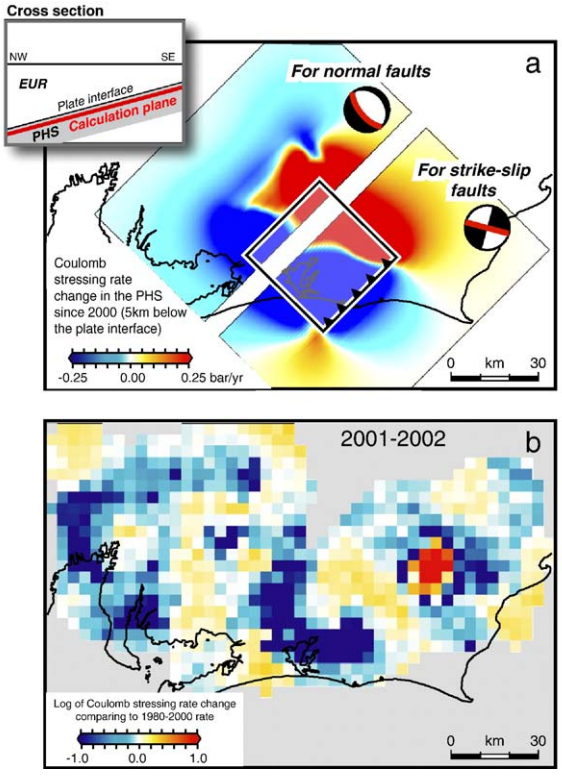


Fig. 11. (a) Composite image of the Coulomb stressing rate changes caused by the slow slip model, resolved on the plane dipping to the northwest below the plate interface. The expected stress shadow is estimated to expand from under Lake Hamana to the northwest. Stress increases to the northeast could have triggered several observed moderate-size shocks. (b) Stressing rate changes inferred from seismicity for the 2000–2004 slow slip event. The observed shadows resemble the model; the stress trigger zone may have been modified by the 2001 $M=5.0$ and 5.4 earthquakes centered on the red zone.

elastically. Matsumura (1999) indeed demonstrates significant extension of the "back-slip" zone to far offshore in his 2D finite element model.

### 5.3. Possible mechanism of stress shadow in slow slip zone

To seek the physical meaning of the inversion results presented in Figs. 3 and 4, we test a simple forward model to explain how aseismic slip perturbs the local stress in the subducting slab. To be consistent with the detailed stress regimes in the down-dip direction (Fig. 6), we calculate the Coulomb stress changes for strike-slip faults in the shallower part, and for normal faults in the deeper part (Fig. 10). Due to the creeping in the plate interface, the Coulomb stress on the typical strike-slip faults directly beneath the creeping patch are calculated to have dropped. Although Coulomb stress for strike-slip faults is estimated to have increased to the down-dip direction, normal faults are moved farther from failure (Fig. 10c). We thus speculate that the primary reason why stress inverted from microseismic-

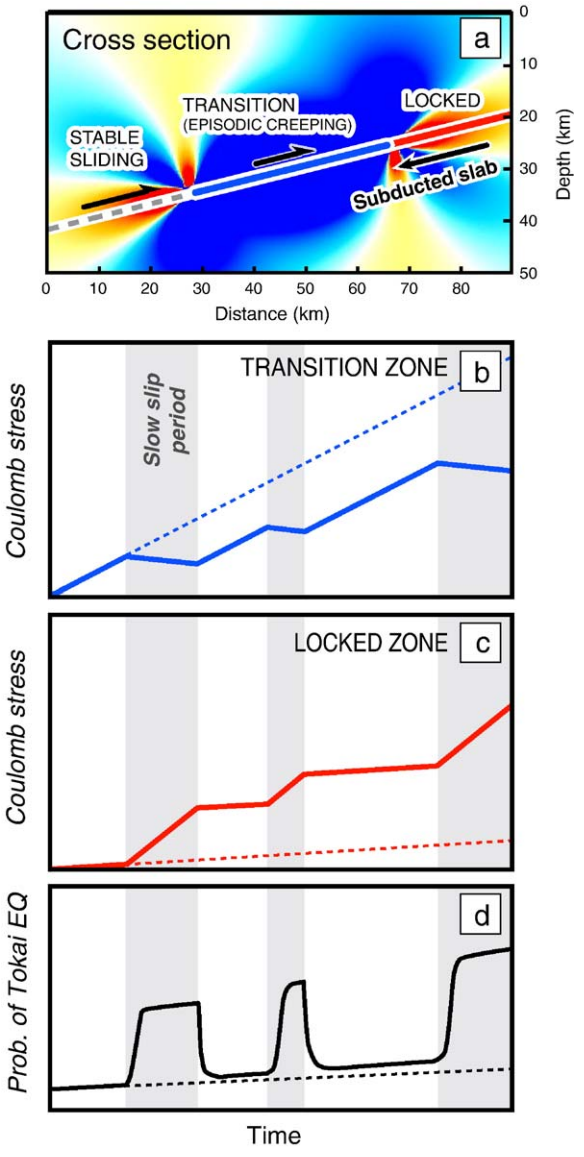


Fig. 12. Schematic process of stress transfer from stable sliding zone, through the transition zone, to the locked zone. (a) Cross-section of stress transferred to the locked zone due to a slow slip event. Warm colors indicate stress increase; cool color indicates stress release. Additional loading to the future source zone of the Tokai earthquake repeatedly occurs with several decades of inter-event time for such slow slip events. (b) Coulomb stress accumulation in the transition zone. The solid line indicates estimated stress fluctuation due to the slow slip events; the dashed line is stress loading without stress perturbations. The shaded areas correspond to periods of slow slip events. (c) Stress in the locked zone. (d) Probability changes associated with the slow slip events.

ity under Lake Hamana (Figs. 3 and 4) has dropped during the slow slip events is due to Coulomb stress transfer. Even though the GPS data suggest that the site of slow slip migrated (Ozawa et al., 2002), the Lake Hamana region has been the center for the various past events. Consequently, the stress shadow tends to locate in and around Lake Hamana (Fig. 11).

### 5.4. Repeating slow slip events

We found the same stress change patterns in the early and late 1980s, as seen in the 2000 Tokai slow slip event. Together with recent discoveries of the repeating silent slip events in the Sagami Trough (Sagiya, 2004), in the western end of the Nankai Trough (Hirose et al., 1999), and in the Cascadian subduction zone (Dragert et al., 2001), we conclude that the 2000 slow slip event is not unique but more likely a repeating event, with the duration of the events longer and less periodic than at least those in Cascadia (Dragert et al., 2001). If slow slip events fit the slip-predictable model (Shimazaki and Nakata, 1980), then the 2000–2004 slow slip event might have a longer duration and larger slip than those in the 1980s because of a longer elapsed time since the last such slip event occurred in the late 1980s.

### 5.5. Stress transfer to locked zone and Tokai probability

Several previous papers regard the recent crustal movement in Tokai region as anomalous and thus precursory to a large earthquake (Matsumura, 2003; Igarashi, 2000; Seno, 2004). Despite our finding of slow slip repeatability in the Tokai region, the 2000s event is the largest, and so could contribute to stress loading of the source region of the next Tokai great earthquake. As shown in Figs. 3 and 4, there is striking evidence that stress is transferred to the surrounding regions, which could have at least triggered a couple of moderate-size shocks in 2001. As schematically shown in Fig. 12a, Coulomb stress is released on the transition zone during the slow slip event, whereas on the locked zone located up-dip, stress is added. Since the stress-transfer is a continuous–rather than abrupt–process, the predicted seismicity rate in rate- and state-friction is expected to have gradually risen with time (Toda et al., 2002). The locked zone might not produce active swarm-like seismicity but the stress transfer may nevertheless increase the likelihood of the Tokai earthquake. Using several equations in Dieterich (1994), the changes in the probability of the Tokai earthquake can be drawn theoretically in Fig. 12d. The probability jumps just after the initiation of slow event but continues to rise over a year or so before reaching the highest probability level. Without knowing the detailed temporal changes of the slip area, the actual probability gain cannot be assessed. But we can nevertheless conclude that the period of slow slip is far more dangerous than normal.

## Acknowledgements

We would like to thank M. Imoto for giving us the opportunity to attend the NIED Kanto-Tokai workshop. We are also indebted to J.H. Dieterich and S. Wiemer for providing their codes for the earthquake-stress inversion and stress tensor inversion analyses. R.S. Stein gave us helpful comments on an earlier draft of the paper. This study was partially supported by SwissRe.

## References

Ando, M., 1975. Source mechanisms and tectonic significance of historic earthquakes along the Nankai trough, Japan. Tectonophysics 27, 119–140.

Angelier, J., 1979. Determination of the mean principal directions of stresses for a given fault population. Tectonophysics 56, T17–T26.

Arrowsmith, R., McNally, K., Davis, J., 1997. Potential for earthquake rupture and M7 earthquakes along the Parkfield, Cholame, and Carrizo segments of the San Andreas fault. Seismol. Res. Lett. 68, 902–906.

Central Disaster Management Council of Japanese government, 2001, Special committee report of the Tokai earthquake, 17 pp. (in Japanese, downloadable PDF file from http://www.bousai.go.jp/jishin/chubou/20011218/siryou2-2.pdf).

Dieterich, J.H., 1994. A constitutive law for rate of earthquake production and its applications to earthquake clustering. J. Geophys. Res. 99, 2601–2618.

Dieterich, J.H., Cayol, V., Okubo, P., 2000. The use of earthquake rate changes as a stress meter at Kilauea volcano. Nature 408, 457–460.

Dragert, H., Wang, K., James, T.S., 2001. A silent slip event on the deeper Cascadia subduction interface. Science 292, 1525–1528.

Geographical Survey Institute, 2004, Seismic activity and the crustal movement of the Tokai district, in Report of the 150th meeting of the Coordinating Committee for Earthquake Prediction (in Japanese but English abstract and figures are available on the web, http://cais.gsi.go.jp/YOCHIREN/ENGLISH/index150.e.html).

Harris, R., 1998. Introduction to special session: stress triggers, stress shadows, and implications for seismic hazard. J. Geophys. Res. 103, 24347–24358.

Harris, R., Simpson, R.W., 1992. Changes in static stress on southern California faults after the 1992 Landers earthquake. Nature 360, 251–254.

Hirose, H., Hirahara, K., Kimata, F., Fujii, N., Miyazaki, S., 1999. A slow thrust slip event following the two 1996 Hyuganada earthquakes beneath the Bungo Channel southwest Japan. Geophys. Res. Lett. 26, 3237–3240.

Igarashi, G., 2000. A geodetic sign of the critical point of stress–stain state at a plate boundary. Geophys. Res. Lett. 27, 1973–1976.

Ishibashi, K., 1976. Reexamination of a great earthquake expected to occur in the Tokai district, central Japan—the great Suruga Bay earthquake. Proc. Fall Meet. Seismol. Soc. Jpn. 30–34 (in Japanese).

Ishibashi, K., 1981. Specification of a soon-to-occur seismic faulting in the Tokai district, central Japan, based upon seismotectonics. Am. Geophys. Union, Maurice Ewing Ser. 4, 297–332.

Jaumé, S.C., Sykes, L.R., 1992. Changes in the state of stress on the southern San Andreas fault resulting from the California earthquake sequence of April to June 1992. Science 258, 1325–1328.

Kato, N., Hirasawa, T., 1999. A model for possible crustal deformation prior to a coming large interplate earthquake in the Tokai district, central Japan. Bull. Seismol. Soc. Am. 89, 1401–1417.

Kimata, F., Hirahara, K., Fujii, N., Hirose, H., 2001. Repeated occurrence of slow slip events on the subducting plate interface in the Tokai region, central Japan, the focal region of the anticipated Tokai earthquake ($M$=8). Eos Trans. AGU, 82, Fall Meeting. Suppl., G31A-0126.

Kuroki, H., Ito, H., Yoshida, A., 2002. A 3-D simulation of crustal deformation accompanied by subduction in the Tokai region, central Japan. Phys. Earth Planet. Inter. 132, 39–58.

Matsumura, S., 1997. Focal zone of a future Tokai earthquake inferred from the seismicity pattern around the plate interface. Tectonophysics 273, 271–291.

Matsumura, S., 1999. Relation between back-slip distribution and locked zone inferred from microearthquake seismicity, Zisin. J. Seismol. Soc. Jpn. 2 (52), 105–108. (in Japanese with English figures and captions).

Matsumura, S., 2003. Spatio-temporal features of the seismicity occurring in the assumed locked area of the next Tokai earthquake. Bull. Earthq. Res. Inst. Univ. Tokyo 78, 269–282. (in Japanese with English abstract and figures).

Michael, A.J., 1987. Use of focal mechanisms to determine stress: a control study. J. Geophys. Res. 92, 357–368.

Ohnaka, 1992. Earthquake source nucleation: a physical model for short-term precursors. Tectonophysics 211, 149–178.

Okada, Y., 1992. Internal deformation due to shear and tensile faults in a half-space. Bull. Seismol. Soc. Am. 82, 1018–1040.

Ozawa, S., Murakami, M., Kaidzu, M., Tada, T., Sagiya, T., Hatanaka, Y., Yarai, H., Nishimura, T., 2002. Detection and monitoring of ongoing aseismic slip in the Tokai region, central Japan. Science 298, 1009–1012.

Reasenberg, P.A., Simpson, R.W., 1992. Response of regional seismicity to the static stress change produced by the Loma-Prieta earthquake. Science 255, 1687–1690.

Sagiya, T., 1999. Interplate coupling in the Tokai District, Central Japan, deduced from continuous GPS data. Geophys. Res. Lett. 26, 2315–2418.

Sagiya, T., 2004. Interplate coupling in the Kanto District, central Japan, and the Boso Silent earthquake in May 1996. Pure Appl. Geophys. 161 (11–12), 2601–2616.

Seno, T., 2004. Intermediate-term precursors of great subduction zone earthquakes: an application for predicting the Tokai earthquake. Earth Planets Space 56, 621–633.

Shimazaki, K., Nakata, T., 1980. Time-predictable recurrence model for large earthquakes. Geophys. Res. Lett. 7, 279–282.

Stein, R.S., 1999. The role of stress transfer in earthquake occurrence. Nature 402, 605–609.

Stein, R.S., King, G.C.P., Lin, J., 1992. Change in failure stress on the southern San Andreas fault system caused by the 1992 Magnitude=7.4 Landers earthquake. Science 258, 1328–1332.

Toda, S., Stein, R.S., 2003. Toggling of seismicity by the 1997 Kagoshima earthquake couplet: a demonstration of time-dependent stress transfer. J. Geophys. Res. 108, 2567. doi:10.1029/2003JB002527.

Toda, S., Stein, R.S., Sagiya, T., 2002. Evidence from the AD 2000 Izu islands earthquake swarm that stressing rate governs seismicity. Nature 419, 58–61.

Ukawa, M., 1982. Lateral stretching of the Philippine Sea plate subducting along the Nankai–Suruga trough. Tectonics 1, 543–571.

Ukawa, M., 1991. Collision and fan-shaped compressional stress pattern in the Izu Block at the northern edge of the Philippine Sea plate. J. Geophys. Res. 96, 713–728.

Wang, K., 2004. “Coupling” semantics and science in earthquake research. EOS 85, 180.

Wiemer, S., 2001. A software package to analyze seismicity: ZMAP. Seismol. Res. Lett. 72, 373–382.

Wiemer, S., Yoshida, A., Hosono, K., Noguchi, S., Takayama, H., 2005. Correlating seismicity and subsidence in the Tokai region, central Japan. J. Geophys. Res. 110, B10303. doi:10.1029/2003JB002732.

Yoshida, A., 2001. Aiming to predict the Tokai earthquake. J. Geogr. 110, 784–807 (in Japanese with English abstract and figures).